The EMBO Journal (2009) 28, 2689–2696 | © 2009 European Molecular Biology Organization | All Rights Reserved 0261-4189/09
www.embojournal.org

THE EMBO JOURNAL

36° step size of proton-driven *c*-ring rotation in F_oF_1-ATP synthase

Monika G Düser[1], Nawid Zarrabi[1], Daniel J Cipriano[2], Stefan Ernst[1], Gary D Glick[3], Stanley D Dunn[2] and Michael Börsch[1,*]

[1]3. Physikalisches Institut, Universität Stuttgart, Stuttgart, Germany, [2]Department of Biochemistry, University of Western Ontario, London, Ontario, Canada and [3]Department of Chemistry, University of Michigan, Ann Arbor, MI, USA

Synthesis of adenosine triphosphate ATP, the 'biological energy currency', is accomplished by F_oF_1-ATP synthase. In the plasma membrane of *Escherichia coli*, proton-driven rotation of a ring of 10 *c* subunits in the F_o motor powers catalysis in the F_1 motor. Although F_1 uses 120° stepping during ATP synthesis, models of F_o predict either an incremental rotation of *c* subunits in 36° steps or larger step sizes comprising several fast substeps. Using single-molecule fluorescence resonance energy transfer, we provide the first experimental determination of a 36° sequential stepping mode of the *c*-ring during ATP synthesis.

The EMBO Journal (2009) **28,** 2689–2696. doi:10.1038/emboj.2009.213; Published online 30 July 2009
Subject Categories: membranes & transport; proteins
Keywords: *c*-ring rotation; F_oF_1-ATP synthase; FRET; single-molecule

Introduction

The difference between the electrochemical potential of ions across a membrane is used by F_oF_1-ATP synthase to catalyse ATP synthesis (Mitchell, 1961). In the current models, proton flux through the membrane-embedded F_o domain causes rotation of its ring of *c* subunits (Elston *et al*, 1998; Aksimentiev *et al*, 2004) with a likely number of 10 for the *Escherichia coli* enzyme (Jiang *et al*, 2001; Ballhausen *et al*, 2009). This rotation is mechanically coupled to rotation of the γ and the ε subunits within F_1, which drives sequential conformational changes in three catalytic binding sites, resulting in the synthesis and release of ATP (Boyer, 1997) (Figure 1A).

Evidence for *c*-ring rotation in single F_oF_1 was reported for the reverse chemical reaction ATP hydrolysis. Using video microscopy of a large fluorescent pointer (Sambongi *et al*, 1999; Sielaff *et al*, 2008) (μm-long actin filaments or polystyrene double-beads), 120° rotations were reported for surface-attached enzymes in the presence of detergent or embedded in lipid bilayer fragments (Nishio *et al*, 2002; Ueno *et al*, 2005). To enable ATP synthesis by ion gradients across the membrane, ion-impermeable lipid vesicles and small markers without viscous drag limitations were used (Kaim *et al*, 2002). However, individual steps during ATP synthesis could not be determined.

We have developed a single-molecule fluorescence resonance energy transfer (FRET) approach for load-free detection of subunit rotation during ATP synthesis in real time (Borsch *et al*, 2002; Diez *et al*, 2004; Zimmermann *et al*, 2005; Duser *et al*, 2008). One fluorophore is attached to a rotor subunit and the second label to a stator subunit in *E. coli* F_oF_1-ATP synthase. On subunit rotation, the proximity of the fluorophores varies with time and anti-correlated changes in the relative fluorescence intensities I_D and I_A of FRET donor and acceptor dye are observed. The distance between dyes is calculated from the time trajectory of the FRET efficiency $E_{FRET} = I_A/(I_A + I_D)$ according to the Förster theory (Forster, 1948). Single-molecule FRET is measured in a confocal microscope setup, in which freely diffusing liposomes generate bursts of photons while traversing the laser focus/detection volume, respectively (Figure 1B). Here, we develop this approach further to unravel the individual step size of *c*-ring rotation and the rotor compliance in the proton-driven F_o motor of F_oF_1-ATP synthase.

Results

Detecting proton-driven c-ring rotation in single F_oF_1-ATP synthases

To deconvolute the sequential stepping of proton-driven *c*-ring rotation, we fused EGFP as FRET donor to the C terminus of the *a* subunit (Duser *et al*, 2008). Alexa568-maleimide was used as a FRET acceptor and was covalently bound to a cysteine (E2C mutation) of one *c* subunit. ATP synthesis activity of this mutant enzyme (27 ATP s^{-1} at 25°C) was slightly reduced by 15% compared with the wild-type enzyme (31 ATP s^{-1} at 25°C). Enzymes were reconstituted singly into liposomes, and ATP synthesis was initiated by mixing two buffers to generate the pH difference and electrical potential across the membrane (Steigmiller *et al*, 2008). Characteristic confocal FRET data from active, single F_oF_1-ATP synthases are shown in Figure 2A–D. To increase the time resolution for a visualization of short rotary steps with dwell times <5 ms, we chose the 'sliding time window FRET analysis' (Margittai *et al*, 2003) and used 50 photons (sum of both FRET donor and acceptor) to calculate one FRET distance data point per 100 μs. The large total fluorescence intensity fluctuations within the photon bursts result from free Brownian motion of the liposome and are caused by the position dependences of excitation power and detection efficiency in the confocal volume. Additionally, the rotational motion of the vesicles in the millisecond time range affects fluorescence excitation and detection efficiencies. However, anti-correlated fluorescence changes clearly indicate intramolecular distance changes due to *c* subunit rotation during

*Corresponding author. 3. Physikalisches Institut, Universität Stuttgart, Pfaffenwaldring 57, Stuttgart 70550, Germany.
Tel.: +49 711 6856 4632; Fax: +49 711 6856 5281;
E-mail: m.boersch@physik.uni-stuttgart.de

Received: 26 March 2009; accepted: 29 June 2009; published online: 30 July 2009

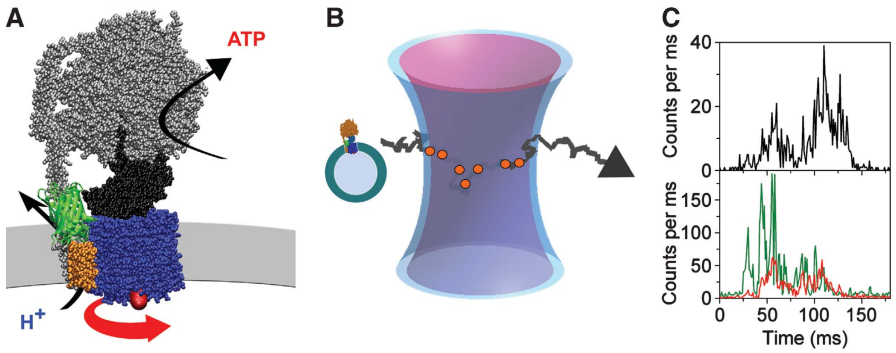

Figure 1 Single-molecule FRET approach to detect the 36° step size of the rotary *c* subunits in F_oF_1-ATP synthase during ATP synthesis. (**A**) Model of FRET-labelled *E. coli* F_oF_1-ATP synthase with EGFP (green; fused to the C terminus of subunit *a*, orange) and Alexa568 (red, at residue E2C) at one of the *c* subunits (blue). Rotation of *c* results in stepwise distance changes to EGFP. (**B**) The FRET-labelled *E. coli* F_oF_1-ATP synthase is reconstituted and diffuses freely through the dual laser foci of the duty cycle-optimized alternating laser excitation scheme. (**C**) Photon burst of a single FRET-labelled F_oF_1-ATP synthase. In the lower panel, fluorescence intensities of FRET donor EGFP (green trace) and acceptor Alexa568 (red trace) are shown excited with 488 nm. In the upper panel, the fluorescence intensity of the directly excited Alexa568 (pulsed interleaved excitation with 561 nm, see text) of the same F_oF_1-ATP synthase is shown (black trace) confirming the existence of both markers on the enzyme.

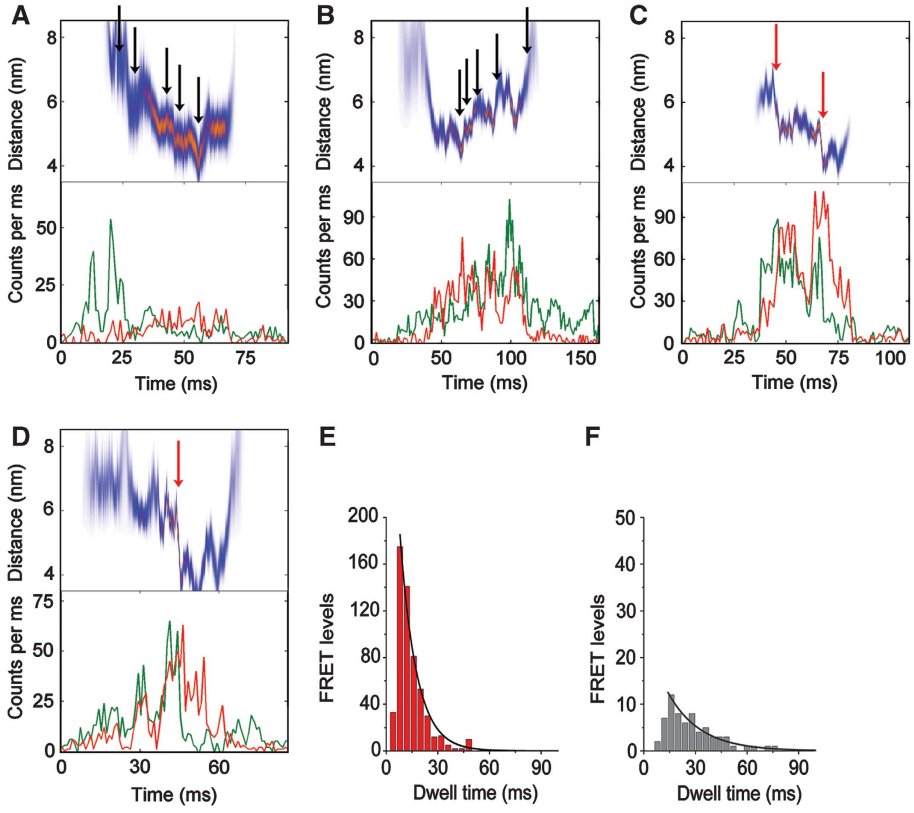

Figure 2 (**A**–**D**) Photon bursts of single FRET-labelled F_oF_1-ATP synthases during ATP synthesis. Lower panels show fluorescence time trajectories for EGFP (green trace) and Alexa568 (red trace), upper panels show the corresponding intramolecular FRET distances (most-likely distance in red and deviations as blue band). Black arrows mark small steps, red arrows large steps. (**E**) Dwell time distributions of FRET levels in F_oF_1-ATP synthases during ATP synthesis (red bars), and (**F**), with 20 μm aurovertin B (gray bars, monoexponential fits in black). Adding an additional rising component apparently improved the fitting at shorter dwells. This is due to the fact that the lower limit to determining dwell times is 2 ms, and thus the histograms lack those data points.

ATP synthesis, which was driven by an initial pH difference from pH 4.7 inside the liposome to pH 8.8 outside in the presence of 100 μM ADP and 5 mM phosphate. About 5 min after generating the pH difference, only few rotating F_oF_1-ATP synthases were detectable because the pH difference was mostly dissipated.

Multiple steps during c-ring rotation

Because of the sub-stoichiometric labelling of the *c* subunit, about 26% of all 11 959 F_oF_1 detected in the sample contained both dyes using continuous-wave laser excitation. Intensity thresholds were applied to identify the double-labelled F_oF_1 in liposomes (for details see Materials and methods below

and Supplementary data). Of these, 14% of the photon bursts showed changes in FRET efficiencies on ATP synthesis, that is, comprised at least two distinguishable FRET levels. In contrast, after incubation with 60 μM DCCD only 5.2% of the bursts with donor and acceptor fluorescence showed FRET fluctuations. The reduced relative number of rotating F_oF_1 corresponded to a residual activity of 37% (or an inhibition efficiency of 63%, respectively). We scrutinized the number of rotating F_oF_1 by an independent FRET measurement applying pulsed alternating laser excitation, ALEX (Kapanidis *et al*, 2004; Muller *et al*, 2005; Zarrabi *et al*, 2007). Each F_oF_1 was excited with a series of 488 nm laser pulses for the FRET measurement, and a subsequent pulse at 561 nm in the same place confirmed the existence of the FRET acceptor fluorophore on the *c* subunit. This variant of alternating excitation optimized the duty cycle for FRET measurement (i.e. called as duty cycle-optimized-ALEX or 'DCO-ALEX'). Sorting the detected photons with respect to the excitation laser pulse yielded two fluorescence time trajectories simultaneously as shown in Figure 1C. About 18–30% of FRET-labelled F_oF_1 showed two and more different FRET states on ATP hydrolysis and ATP synthesis, but in the presence of the non-hydrolysable ATP derivative AMPPNP only 2.5% of F_oF_1 exhibited two different FRET states (summarized in the Supplementary data).

The FRET efficiency changes from step to step were smaller than found earlier for the case of γ or ε subunit rotation (Diez *et al*, 2004; Zimmermann *et al*, 2005; Duser *et al*, 2008). Sometimes up to five FRET levels occurred in a series. Black arrows in Figure 2A and B are positioned to highlight those FRET distance levels that differ slightly but in a sequential order with decreasing or increasing distances. The distances were spanning the maximum expected range for distance changes during *c* rotation. However, apparently larger step sizes were observed also (see Figure 2C and D). Here, the red arrows point towards the transitions between the two distances, which were obviously larger than those found in the other two examples of F_oF_1 photon bursts. Forward–backward fluctuating steps with small distance changes were found in many photon bursts, which could be interpreted in support of the Brownian Ratchet Model for proton-driven *c*-ring rotation (Elston *et al*, 1998) and a rotor compliance (Sielaff *et al*, 2008; Junge *et al*, 2009).

Affecting dwell times of rotating c subunits with aurovertin B

As FRET level changes were assigned manually at first, we subsequently applied intensity thresholds to the FRET data set to verify that all marked FRET levels consisted of only one FRET level with limited standard deviation from its mean distance (see Supplementary data). From the remaining FRET levels, the intermediary FRET levels without the first and the last level of the photon burst were selected. Their dwell times were binned to 4 ms time intervals yielding the distribution shown in Figure 2E. The average dwell time was determined to 9 ± 1 ms by fitting the histogram with one decay component. This value is much shorter than the 18–51 ms dwell times found for the γ or ε subunits in F_oF_1, which rotate in 120° steps (Diez *et al*, 2004; Zimmermann *et al*, 2005). Assuming that one proton is transported with each *c* subunit step (i.e. 111 protons/s) and that four protons have to be translocated across the membrane for each ATP (Steigmiller *et al*, 2008), an ATP synthesis rate of 28 s^{-1} can be calculated from the single-molecule FRET data measured at 20°C. This rate is in accordance with the biochemical measurements.

To validate the rotational speed of the *c*-ring, we added a non-competitive inhibitor of ATP synthesis. In the presence of 20 μM of the inhibitor aurovertin B (Satre *et al*, 1978), which binds to β in the F_1 part (Dunn and Futai, 1980; van Raaij *et al*, 1996), the relative number of ATP synthases with rotating *c* subunits was reduced by 74% (calculated from the number of F_oF_1 with two and more FRET levels in Supplementary Table II). In addition, the dwell times were prolonged more than two-fold; fitting yielded a decay component of 19 ± 2 ms (Figure 2F). For ATP hydrolysis conditions in the presence of 1 mM ATP, the mean dwell time for *c*-ring rotation was 13 ± 1 ms (Supplementary Figure S5A). Adding 20 μM aurovertin B also slowed down rotation during ATP hydrolysis consistent with earlier measurements (Johnson *et al*, 2009). The relative number of rotating F_oF_1-ATP synthases was reduced, but only by 27% (Supplementary Figure S5B; Supplementary Table II). Fitting the dwells required two exponentials and resulted in a rising time component of 6 ms and a decay component of 18 ms. Thus, aurovertin B reduced the rotational speed during ATP hydrolysis by a factor of 2, or to a remaining activity of about 50%. Aurovertin B affects ATP synthesis as well as ATP hydrolysis causing a slow-down of *c*-ring rotation. These results excluded photophysical artifacts like spectral fluctuations of EGFP (Duser *et al*, 2006) as the cause for the short dwell times and the multiple steps seen in Figure 2.

Small step sizes of rotating c subunits

To determine the step size of *c*-ring rotation during ATP synthesis, we calculated the distance between the fluorophores on F_oF_1 for each FRET level and plotted FRET distance 1 against the subsequent FRET distance 2 in the FRET transition density plot (McKinney *et al*, 2006) Two models were considered that had to be discriminated by this plot: model I expected 120° stepping for *c* as deduced from the step size of the γ and ε subunits. Model II anticipated individual step sizes of 36° as expected from the 10-fold symmetry of the *c*-ring and the assumption that each *c* subunit passes the stator individually. The geometric models are shown in Figure 3A–C. The chromophore of the FRET donor EGFP was localized earlier by single-molecule FRET triangulation on the cytosolic side near the membrane level of the F_o part of F_oF_1-ATP synthase and the FRET acceptor was attached to residue 2 on the *c* subunit on the periplasmic side of the membrane (Duser *et al*, 2008). Accordingly, we estimated the limits for the distances to be measured during full rotation of *c*. The constraints were (1) a radius of the FRET acceptor rotation for 2.5 nm on the *c*-ring; (2) the chromophore within EGFP located 3.2 nm off the axis of rotation and (3) 4.2 nm above the plane of Alexa568 rotation. Given the Förster radius $R_0 = 4.9$ nm (Duser *et al*, 2008), this yielded the possible transitions for the case of 36° stepping (Figure 3D) shown as the white curve and 120° stepping (Figure 3E) shown as the black curve in Figure 3F. Many FRET transitions were located near the diagonal, and the maxima in the histogram matched the curve for 36° steps. Some transitions were detected apart from the curve for 36° steps but this can be explained by apparent larger step sizes due to unassigned short steps. The experimental data for *c*-ring rotation during

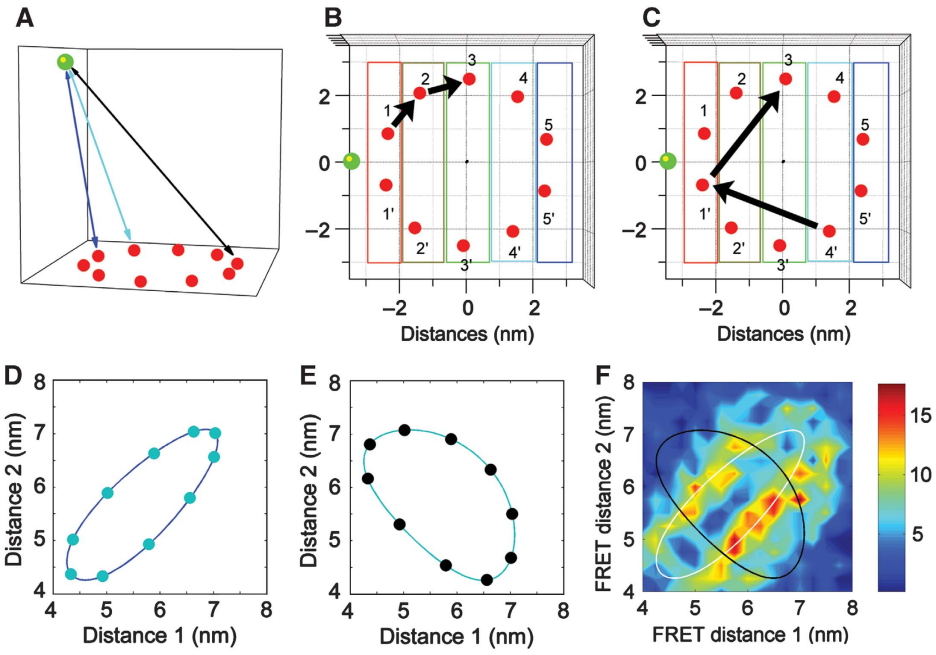

Figure 3 Model for the geometrical constraints for the FRET measurements within a single F_oF_1-ATP synthase and FRET transition density plot. (**A**) Model for FRET distances between the EGFP chromophore (green dot) and three of the 10 stopping positions of Alexa568 (red dots) during *c*-ring rotation. Distance changes for a 36° step correspond to arrows blue and cyan; a 144° step corresponds to arrows blue and black. (**B**) Five zones for the 10 *c* positions as defined from symmetry reasons. 36° stepping of *c* results in changing between adjacent zones, and, correspondingly, incremental FRET distance changes. (**C**) Larger step sizes of 108° require switching between non-neighbouring zones. (**D**) Transitions between FRET distances according to 36° steps and geometries as shown in panel B. (**E**) Transitions between FRET distances according to 120° steps. (**F**) FRET transition density plot for proton-driven *c* subunit rotation with constraint curves for 36° steps in white and for 120° steps in black.

ATP hydrolysis are shown in Supplementary Figure S5C (and examples of photon bursts in Supplementary Figure S6C and D). Many data points were associated with the ellipse describing a 36° stepping mode. However, other FRET transition data points could be interpreted to support the earlier reported 120° stepping in detergent-solubilized F_oF_1.

Identifying 36° steps of the c-ring

The aim was to quantify the probability for 36° step size of *c*-ring rotation according to the qualitative analysis of FRET transition distribution in Figure 3F. FRET measured the distance from the static EGFP chromophore to one of the 10 possible positions of the step-wise rotating Alexa568. For symmetry reasons, the anticipated *c* stopping positions were subdivided into five zones within the plane of rotation (as seen from below in Figure 3B and C), with boundaries at 4.6, 5.4, 6.2 and 6.8 nm. The lower limit was set to 4.1 nm and the upper limit was set to 7.3 nm. All FRET distances were assigned to one of the five zones, and the step size was estimated according to transitions between these zones. For example, in Figure 3B positions 1, 2 and 3 were assigned to three different but adjacent distance intervals, and a FRET distance sequence in this order corresponds to 36° stepping. *Vice versa*, a FRET distance sequence for positions $4' \rightarrow 1' \rightarrow 3$ as shown in Figure 3C corresponds to 108° stepping. However, positions 1 and 1′ both correspond to distances between 4.1 and 4.6 nm, that is, they are indistinguishable and belong to the same FRET level. Accordingly, the stepping sequences of three subsequent experimental FRET distances were analysed. If one distance change could be assigned to two different step sizes, the smaller step size was taken into account. Analysing all data points for ATP synthesis conditions (i.e. 1879 FRET level pairs in the FRET transition density plot shown as Figure 3F) resulted in 48% of transitions according to 36° stepping, 37% according to 72° stepping, 12% according to 108° stepping and 3% according to 144° stepping. For ATP hydrolysis conditions (912 steps in Supplementary Figure S5C) 36° stepping was associated with 23% of all FRET level transitions.

Simulating the 36° step size distribution

The reliability of this step size assignment was assessed by simulations of *c*-ring rotation for all step sizes. To access the step size from FRET distance measurements during ATP synthesis, we plotted the absolute value of the differences in the FRET distances |distance1–distance2| in Figure 4. The histograms from 1879 distance pairs had its maximum at distances changes around 0.8 nm (Figure 4A). Assuming 36° (or other step sizes, respectively), this distribution was simulated using a Monte Carlo approach with the same limited number of distance pairs and the geometrical constraints for *c*-ring rotation. For each distance, a standard error according to the shot-noise limit was assumed in the simulation, that is, about 0.5 nm. For the case of 36° step size only, the FRET distance difference histogram reproduced short differences very well but was insufficient for the small number of differences corresponding to larger step sizes (Figure 4B). *Vice versa*, for the cases of larger step sizes (Figure 4C–F), the FRET distance difference histogram did not reproduce the number of short differences correctly.

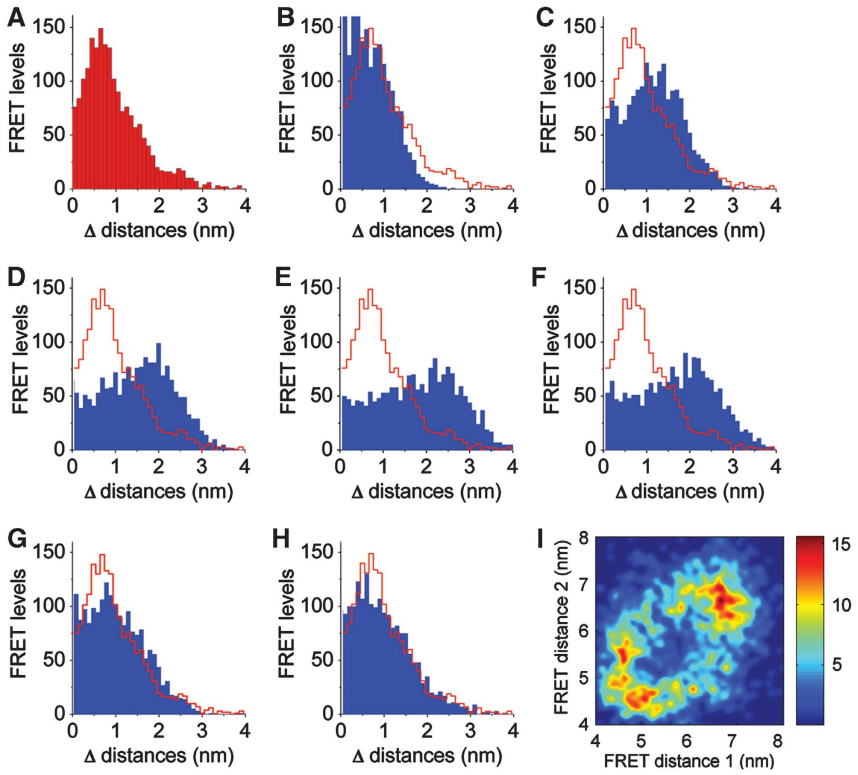

Figure 4 Monte Carlo simulations of FRET distance changes during stepwise *c*-ring rotation and comparison with experimental data during ATP synthesis. (**A**) Experimental FRET distance changes. Simulations with 36° (**B**), 72° (**C**), 108° (**D**), 144° (**E**), 120° (**F**), 40° plus 80° (**G**); the weighted sum of 36°, 72°, 108° and 144° step sizes (**H**) reproduced the FRET distance difference plot and the experimental FRET transition density plot (see Figure 3F) fairly well. **I**, FRET transition density plot from the Monte Carlo simulation shown in (H).

Importantly, the FRET distance difference histogram could not be reproduced using the 120° step size (Figure 4F). Assuming alternating 40° and 80° steps as reported for the γ subunit in thermophilic F_1 parts (Yasuda *et al*, 2001) improved the simulated FRET distance histogram (Figure 4G) but slightly overestimated the occurrence of larger distance changes. The best solution according to the Monte Carlo simulations was the weighted mixture of 36° (48%), 72° (37%), 108° (12%) and 144° (3%) steps (Figure 4H) as extracted from the FRET stepping analysis described in the earlier paragraph. The corresponding FRET transition density plot in Figure 4I is in good agreement with the experimental data.

Likelihood of 36° step size

The number of consecutive 36° steps was usually low. Only 138 of 1879 FRET transition pairs were unequivocally assigned to two 36° successive steps, that is, showing a sequence of two stopping positions in adjacent zones according to Figure 3B. This might be due to the limited time resolution of manual FRET transition assignment and the subsequently applied thresholds. The fastest time interval for 120° stepping of the γ and ε subunit in F_1 during ATP synthesis, that is, three to four steps for the proton-driven *c*-ring, has been estimated to be as fast as 200μs (Zimmermann *et al*, 2006). Considering a mean dwell time of 9 ms for each *c*-ring FRET position during ATP synthesis and a minimal length of 5 ms for a FRET level to be identified and discriminated from the earlier and subsequent level, the probability of over-looking short FRET levels reaches 49%, with likelihoods of missing one or two steps of 25 and 12%, respectively. Furthermore, transitions between some positions in particular 1–1′, or 5–5′ (Figure 3B) cannot be assigned as they result in no significant change in distance. Accordingly, the experimental FRET transition density plot in Figure 3F lacks the clustered transitions at the largest and shortest distances compared with the simulated data in Figure 4I.

Discussion

Early models of *c*-ring rotation considered the F_o sector in isolation and predicted a step size inversely proportional to the number of *c* subunits, for example, 36° for the 10-membered *c*-rings of *E. coli* or yeast mitochondria (Elston *et al*, 1998; Aksimentiev *et al*, 2004). More recent models of *c*-ring rotation in the holoenzyme, that is, with a tightly coupled F_1 part stepping in 120°, predict different step sizes in multiples of 36° depending on the shape of the torque profile and the number of *c* subunits in F_o (Jun *et al*, 2005). This depends, however, on the rigidity of the γε rotor and $b_2\delta$ stator stalk that link F_o and F_1. If these elements function as rigid bodies, subsequent 36° steps were not expected to occur for a c_{10}-ring (Jun *et al*, 2005). Hence, our findings of consecutive 36° steps during ATP synthesis indicate a high elasticity, consistent with the results obtained recently for the detergent-solubilized enzyme with an attached bead as a load (Sielaff *et al*, 2008). This elasticity allows the storage of energy released from the transmembrane movement of several H^+ to be stored for the synthesis of a single ATP.

In summary, our single-molecule FRET measurements reveal a step-by-step rotary motion of the *c* subunit ring in 36° steps during proton-driven ATP synthesis. This result provides experimental support for the concept that, as each subunit of the decameric *c*-ring rotates past the *a* subunit, one H^+ is translocated, winding up the elastic element(s) of the enzyme, most likely the globular region of the γ subunit located between the *c*-ring and the $\alpha_3\beta_3$ catalytic domain (Sielaff *et al*, 2008; Junge *et al*, 2009). We can detect this step-by-step motion most clearly during ATP synthesis because successive steps were slowed by the conservation of energy during this process. Further studies aim to provide insight into energy storage in the system and into how the symmetry mismatch between $\alpha_3\beta_3$ and the *c*-ring stoichiometry, present in F_oF_1-ATP synthase from most species, affects sequential steps of ATP synthesis.

Materials and methods

FRET-labelled F_oF_1-ATP synthase

Construction of plasmids carrying an E2C mutation in the c subunit. Plasmid pDC60 is a derivative of pACWU1.2 (Kuo *et al*, 1998) carrying an E2C mutation in the *c* subunit. Plasmid pDC61 carries a fusion of EGFP to the C terminus of the *a* subunit, derived from plasmid pSD166 (Duser *et al*, 2008), as well as the E2C mutation in the *c* subunit. A segment of DNA encoding the E2C mutation was produced by primed synthesis from a pair of annealed primers, 5′-GAAACAAACTG**GAGAC**TGTCATGTGTAACCTG and 5′-GCCA**TGTACA**GCAGATCCATATTCAGGTTACACATG, in which the nucleotides in bold provide cleavage sites for restriction endonucleases BsmAI and BsrGI, respectively. The product was cut with those two enzymes and combined with the 8451-bp PflMI/BsrG1 fragment of pACWU1.2 and the 745-bp BsmAI/PflMI fragment of pVF172 (Valiyaveetil and Fillingame, 1998) in a three-part ligation to produce plasmid pDC60. Another portion of the digested product of primed synthesis was combined with the 8451-bp PflMI/BsrG1 fragment of pACWU1.2 and the 1478-bp BsmAI/PflMI piece from plasmid pSD166 to produce plasmid pDC61. Correct plasmid sequences were confirmed by restriction endonuclease mapping and by DNA sequencing.

Expression, purification and labelling of F_oF_1-ATP synthase. F_oF_1-ATP synthase carrying the EGFP fusion protein plus the *c*E2C mutation was prepared as described (Diez *et al*, 2004; Zimmermann *et al*, 2005) after expressing plasmid pDC61 in strain RA1 (Aggeler *et al*, 1997). Specific labelling of *c*E2C with Alexa568-maleimide (Molecular Probes) was carried out with detergent-solubilized enzymes using a sub-stoichiometric labelling efficiency of about 25% for one *c* subunit. The specificity of the labelling was checked by fluorogram analysis of an SDS–PAGE gel. F_oF_1 was reconstituted into preformed liposomes (diameter ∼120 nm) resulting in membrane-integrated F_oF_1 labelled with both the FRET donor, EGFP and the acceptor, Alexa568, which were stored at −80°C.

Rates of ATP synthesis and hydrolysis were measured at room temperature (25°C) as described earlier (Diez *et al*, 2004; Zimmermann *et al*, 2005; Duser *et al*, 2008). To synthesize ATP, a pH transition was performed from pH 4.7 to pH 8.8 in the presence of 100 μM ADP and 5 mM phosphate. On addition of 60 μM DCCD, ATP synthesis activity of reconstituted F_oF_1-ATP synthase was nearly abolished.

Confocal setup with duty cycle-optimized alternating laser excitation

Confocal single-molecule FRET measurements using continuous-wave excitation. The single-molecule measurements were carried out on a custom-built confocal microscope as described (Duser *et al*, 2008; Zarrabi *et al*, 2009). Briefly, proteoliposomes were excited continuously at 488 nm (argon ion laser, model 2020, Spectra Physics). The laser beam was attenuated to 150 μW on the back aperture of the microscope objective and focussed by a water immersion objective (UPlanSApo 60×, N.A. 1.2, Olympus) into a droplet of buffer solution placed on a microscope coverslide. The fluorescence emission was separated from the excitation light by a dichroic beam splitter (c488RDC, AHF, Tübingen, Germany). Emission of the two fluorophores was split by a second dichroic beamsplitter (HQ 575, AHF Germany). Single photons were detected separately by two avalanche photodiodes (SPCM-AQR-14, EG&G, Canada) after passing an interference filter (HQ 532/70, AHF) for EGFP, or a long pass filter (LP595, AHF) for Alexa568. Detection efficiencies were $\eta_D = 0.36$ for EGFP and $\eta_A = 0.40$ for Alexa568. A cross-talk of 0.3% from donor fluorescence in the acceptor channel was neglected. Photons were counted by a TCSPC card (SPC630, Becker&Hickl, Germany) in FIFO mode with 50 ns time resolution using the router electronics (HRT-82, Becker&Hickl) to assign the FRET channel information for each photon.

Confocal single-molecule FRET measurements using pulsed, duty cycle-optimized, alternating laser excitation at 488 and 561 nm (DCO-ALEX). A second, independent set of single-molecule FRET data were recorded using picosecond 488 nm pulses (PicoTA490; Picoquant, Germany) and alternating pulses at 561 nm (Jive; Cobolt, Sweden), which were switched by an fast acousto-optical modulator as described (Zarrabi *et al*, 2007) (Supplementary Figure S1). Both laser beams were overlaid and re-directed to the objective by a dual-band beam splitter (HC dichroic 488/561–568, AHF). Lasers were triggered externally by an arbitrary waveform generator (AWG 2041, Tektronix, USA) to obtain a sequence of six pulses at 488 nm separated by 12 ns. These were followed by one 561 nm pulse with 12 ns duration (Supplementary Figure S1). Thereby, the excitation probability of the FRET donor EGFP was optimized and reached a duty cycle of 75% (DCO-ALEX) compared with the maximum repetition rate of 83.3 MHz for the 488 nm laser alone.

Fluorescence was detected in the two spectral ranges, that is, from 500 to 550 nm for EGFP and from 575 to 648 nm for Alexa568, with detection efficiencies $\eta_D = 0.32$ for EGFP and $\eta_A = 0.38$ for Alexa568. A cross-talk of 11.4% from donor fluorescence in the acceptor channel was corrected. Photon counting with synchronized TCSPC electronics (SPC152, Becker&Hickl, Germany) provided the arrival time for FRET donor lifetime determination with picosecond time resolution. The EGFP fluorescence lifetimes per FRET level were plotted against the EGFP/Alexa568 intensity ratio (Antonik *et al*, 2006) to prove that the intensity ratio corresponds to FRET (Supplementary Figure S4). Fluorophore mobilities of both FRET labels on individual F_oF1-ATP synthase were measured by burst-wise single-molecule anisotropy (Supplementary Figure S2) and $\kappa^2 = 2/3$ was assumed for the FRET distance calculations. The distance error was estimated to be $<20\%$ when calculated as described (Dale *et al*, 1979).

Single-molecule FRET data analysis

Photon burst analysis. Single photon bursts were detected as FRET-labelled F_oF_1-ATP synthases freely diffused through the confocal detection volume. To identify a single burst from background, a minimum count rate threshold for each of the two detection channels was applied (10 counts per ms). In case of alternating excitation, search for FRET-labelled enzymes was based on a minimum count rate threshold (5 counts per ms) for the directly excited Alexa568, plus a minimum threshold for the sum of both FRET donor and acceptor intensities.

Within a single burst, changes in the relative fluorescence intensities of the two fluorophores are due to varying proximity of the FRET pair, that is, indicate *c*-ring rotation. The steps were identified from changes in the relative intensities and assigned manually using 1-ms time binning. Step sizes varied from burst to burst and from small changes to larger steps as shown in Figure 2A–D for ATP synthesis conditions (see also Supplementary Figure S6). To improve the time resolution, a 50-photon 'sliding time window' (Margittai *et al*, 2003) was applied for calculating the FRET distance within selected photon bursts. Thus, photon bursts with high count rates revealed fast stepping of *c*-ring rotation. At this higher time resolution, fluctuations or small forward–backward steps could be identified.

FRET distance analysis. To calculate the actual distance between the fluorophores from the FRET efficiency, we used background- and crosstalk-corrected intensities I_D and I_A to calculate the

proximity factor P

$$P = \frac{I_A}{I_A + I_D} \quad (1)$$

The calibration factor γ incorporates the different quantum yields ϕ_D and ϕ_A of the fluorophores and the different detection efficiencies η_D and η_A,

$$\gamma = \frac{\phi_A \, \eta_A}{\phi_D \, \eta_D} \quad (2)$$

The FRET efficiency E_{FRET} is given by

$$E_{FRET} = \frac{I_A}{I_A + \gamma I_D} \quad (3)$$

The absolute donor–acceptor distance d is calculated using the Förster radius R_0 and the γ factor

$$d = R_0 \, \gamma^{1/6} \left(\frac{1}{P} - 1 \right)^{1/6} \quad (4)$$

However, the Poissonian character of the measured fluorescence intensities yields a shot noise-broadened proximity factor, which can be described by a beta distribution (McKinney *et al*, 2006):

$$P(x) = \frac{1}{B(I_A, I_D)} x^{I_A - 1} (1 - x)^{I_D - 1} \quad (5)$$

with x values between 0 and 1, and a normalization factor $B(I_A, I_D)$. The mean value μ_P for P is

$$\mu_P = \frac{I_A}{I_D + I_A} \quad (6)$$

with a standard deviation σ_P

$$\sigma_P = \sqrt{\frac{I_A I_D}{(I_D + I_A)^2 (I_D + I_A - 1)}} \quad (7)$$

The $2\sigma_P$ borders $P_{1/2} = \mu_P \pm \sigma_P$ can be obtained by the inverted cumulative beta distribution function (Supplementary Figure S3).

Supplementary data

Supplementary data are available at *The EMBO Journal* Online (http://www.embojournal.org).

Acknowledgements

We thank P Gräber and coworkers (University of Freiburg) for their help in enzyme purification and J Wrachtrup (University of Stuttgart) for supporting the development of the confocal setup. Financial support from the Deutsche Forschungsgemeinschaft (grant BO 1891/10-1 to MB), the Landesstiftung Baden-Württemberg, the Canadian Institutes of Health Research (grant MOP-10237 to SDD), and the NIH (grant RO1-AI 47450 to GDG) is gratefully acknowledged.

Conflict of interest

The authors declare that they have no conflict of interest.

References

Aggeler R, Ogilvie I, Capaldi RA (1997) Rotation of a gamma-epsilon subunit domain in the Escherichia coli F1F0-ATP synthase complex. The gamma-epsilon subunits are essentially randomly distributed relative to the alpha3beta3delta domain in the intact complex. *J Biol Chem* **272:** 19621–19624

Aksimentiev A, Balabin IA, Fillingame RH, Schulten K (2004) Insights into the molecular mechanism of rotation in the F-o sector of ATP synthase. *Biophys J* **86:** 1332–1344

Antonik M, Felekyan S, Gaiduk A, Seidel CA (2006) Separating structural heterogeneities from stochastic variations in fluorescence resonance energy transfer distributions via photon distribution analysis. *J Phys Chem B* **110:** 6970–6978

Ballhausen B, Altendorf K, Deckers-Hebestreit G (2009) Constant c(10) ring stoichiometry in the Escherichia coli ATP synthase analyzed by cross-linking. *J Bacteriol* **191:** 2400–2404

Borsch M, Diez M, Zimmermann B, Reuter R, Graber P (2002) Stepwise rotation of the gamma-subunit of EF(0)F(1)-ATP synthase observed by intramolecular single-molecule fluorescence resonance energy transfer. *FEBS Lett* **527:** 147–152

Boyer PD (1997) The ATP synthase—a splendid molecular machine. *Annu Rev Biochem* **66:** 717–749

Dale RE, Eisinger J, Blumberg WE (1979) The orientational freedom of molecular probes. The orientation factor in intramolecular energy transfer. *Biophys J* **26:** 161–193

Diez M, Zimmermann B, Borsch M, Konig M, Schweinberger E, Steigmiller S, Reuter R, Felekyan S, Kudryavtsev V, Seidel CA, Graber P (2004) Proton-powered subunit rotation in single membrane-bound F0F1-ATP synthase. *Nat Struct Mol Biol* **11:** 135–141

Dunn SD, Futai M (1980) Reconstitution of a functional coupling factor from the isolated subunits of Escherichia coli F1 ATPase. *J Biol Chem* **255:** 113–118

Duser MG, Bi Y, Zarrabi N, Dunn SD, Borsch M (2008) The proton-translocating a subunit of F0F1-ATP synthase is allocated asymmetrically to the peripheral stalk. *J Biol Chem* **283:** 33602–33610

Duser MG, Zarrabi N, Bi Y, Zimmermann B, Dunn SD, Borsch M (2006) 3D-localization of the a-subunit in FoF1-ATP synthase by time resolved single-molecule FRET. *Proc of SPIE* **6092:** 60920H; doi:10.1117/12.647988

Elston T, Wang H, Oster G (1998) Energy transduction in ATP synthase. *Nature* **391:** 510–513

Forster T (1948) Zwischenmolekulare Energiewanderung Und Fluoreszenz. *Annalen Der Physik* **2:** 55–75

Jiang W, Hermolin J, Fillingame RH (2001) The preferred stoichiometry of c subunits in the rotary motor sector of Escherichia coli ATP synthase is 10. *Proc Natl Acad Sci USA* **98:** 4966–4971

Johnson KM, Swenson L, Opipari Jr AW, Reuter R, Zarrabi N, Fierke CA, Borsch M, Glick GD (2009) Mechanistic basis for differential inhibition of the F(1)F(o)-ATPase by aurovertin. *Biopolymers*; doi:10.1002/bip.21262

Jun Q, Ping X, Dou SX, Wang PY (2005) Numerical study of the coupling between F-0 with varied numbers of c-subunits and F-1 in an ATP synthase. *Chinese Phys* **14:** 2214–2221

Junge W, Sielaff H, Engelbrecht S (2009) Torque generation and elastic power transmission in the rotary FOF1-ATPase. *Nature* **459:** 364–370

Kaim G, Prummer M, Sick B, Zumofen G, Renn A, Wild UP, Dimroth P (2002) Coupled rotation within single F0F1 enzyme complexes during ATP synthesis or hydrolysis. *FEBS Lett* **525:** 156–163

Kapanidis AN, Lee NK, Laurence TA, Doose S, Margeat E, Weiss S (2004) Fluorescence-aided molecule sorting: analysis of structure and interactions by alternating-laser excitation of single molecules. *Proc Natl Acad Sci USA* **101:** 8936–8941

Kuo PH, Ketchum CJ, Nakamoto RK (1998) Stability and functionality of cysteine-less F(0)F1 ATP synthase from Escherichia coli. *FEBS Lett* **426:** 217–220

Margittai M, Widengren J, Schweinberger E, Schroder GF, Felekyan S, Haustein E, Konig M, Fasshauer D, Grubmuller H, Jahn R, Seidel CAM (2003) Single-molecule fluorescence resonance energy transfer reveals a dynamic equilibrium between closed and open conformations of syntaxin 1. *Proc Natl Acad Sci USA* **100:** 15516–15521

McKinney SA, Joo C, Ha T (2006) Analysis of single-molecule FRET trajectories using hidden Markov modeling. *Biophys J* **91:** 1941–1951

Mitchell P (1961) Coupling of phosphorylation to electron and hydrogen transfer by a chemi-osmotic type of mechanism. *Nature* **191:** 144–148

Muller BK, Zaychikov E, Brauchle C, Lamb DC (2005) Pulsed interleaved excitation. *Biophys J* **89:** 3508–3522

Nishio K, Iwamoto-Kihara A, Yamamoto A, Wada Y, Futai M (2002) Subunit rotation of ATP synthase embedded in membranes: a or beta subunit rotation relative to the c subunit ring. *Proc Natl Acad Sci USA* **99:** 13448–13452

Sambongi Y, Iko Y, Tanabe M, Omote H, Iwamoto-Kihara A, Ueda I, Yanagida T, Wada Y, Futai M (1999) Mechanical rotation of the c subunit oligomer in ATP synthase (F0F1): direct observation. *Science* **286:** 1722–1724

Satre M, Klein G, Vignais PV (1978) Isolation of Escherichia coli mutants with an adenosine triphosphatase insensitive to aurovertin. *J Bacteriol* **134:** 17–23

Sielaff H, Rennekamp H, Wachter A, Xie H, Hilbers F, Feldbauer K, Dunn SD, Engelbrecht S, Junge W (2008) Domain compliance and elastic power transmission in rotary F(O)F(1)-ATPase. *Proc Natl Acad Sci USA* **105:** 17760–17765

Steigmiller S, Turina P, Graber P (2008) The thermodynamic H + /ATP ratios of the H + -ATPsynthases from chloroplasts and Escherichia coli. *Proc Natl Acad Sci USA* **105:** 3745–3750

Ueno H, Suzuki T, Kinosita Jr K, Yoshida M (2005) ATP-driven stepwise rotation of FoF1-ATP synthase. *Proc Natl Acad Sci USA* **102:** 1333–1338

Valiyaveetil FI, Fillingame RH (1998) Transmembrane topography of subunit a in the Escherichia coli F1F0 ATP synthase. *J Biol Chem* **273:** 16241–16247

van Raaij MJ, Abrahams JP, Leslie AG, Walker JE (1996) The structure of bovine F1-ATPase complexed with the antibiotic inhibitor aurovertin B. *Proc Natl Acad Sci USA* **93:** 6913–6917

Yasuda R, Noji H, Yoshida M, Kinosita Jr K, Itoh H (2001) Resolution of distinct rotational substeps by submillisecond kinetic analysis of F1-ATPase. *Nature* **410:** 898–904

Zarrabi N, Duser MG, Ernst E, Reuter R, Glick GD, Dunn SD, Wrachtrup J, Borsch M (2007) Monitoring the rotary motors of single F_0F_1-ATP synthase by synchronized multi channel TCSPC. *Proc SPIE* **6771:** 67710F; doi:10.1117/12.734301

Zarrabi N, Ernst S, Duser MG, Golovina-Leiker A, Becker W, Erdmann R, Dunn SD, Borsch M (2009) Simultaneous monitoring of the two coupled motors of a single F[sub o]F[sub 1]-ATP synthase by three-color FRET using duty cycle-optimized triple-ALEX. *Proc SPIE* **7185:** 718505; doi:10.1117/12.809610

Zimmermann B, Diez M, Borsch M, Graber P (2006) Subunit movements in membrane-integrated EF0F1 during ATP synthesis detected by single-molecule spectroscopy. *Biochimica et Biophysica Acta* **1757:** 311–319

Zimmermann B, Diez M, Zarrabi N, Graber P, Borsch M (2005) Movements of the epsilon-subunit during catalysis and activation in single membrane-bound H(+)-ATP synthase. *EMBO J* **24:** 2053–2063

